Quantum Memory for Microwave Photons in an Inhomogeneously Broadened Spin Ensemble

Brian Julsgaard,[1,*] Cécile Grezes,[2] Patrice Bertet,[2] and Klaus Mølmer[1]

[1]Department of Physics and Astronomy, Aarhus University, Ny Munkegade 120, DK-8000 Aarhus C, Denmark
[2]Quantronics group, SPEC (CNRS URA 2464), IRAMIS, DSM, CEA-Saclay, 91191 Gif-sur-Yvette, France

(Received 8 January 2013; published 18 June 2013)

We propose a multimode quantum memory protocol able to store the quantum state of the field in a microwave resonator into an ensemble of electronic spins. The stored information is protected against inhomogeneous broadening of the spin ensemble by spin-echo techniques resulting in memory times orders of magnitude longer than previously achieved. By calculating the evolution of the first and second moments of the spin-cavity system variables for current experimental parameters, we show that a memory based on nitrogen vacancy center spins in diamond can store a qubit encoded on the $|0\rangle$ and $|1\rangle$ Fock states of the field with 80% fidelity and outperform classical memory strategies for storage times $\leq 69\ \mu$s.

DOI: 10.1103/PhysRevLett.110.250503 PACS numbers: 03.67.Lx, 42.50.Ct, 42.50.Pq, 71.55.Cn

Quantum memories are indispensable in quantum information applications such as quantum repeaters and hybrid quantum computing architectures. The study of quantum memories [1] is hence a very active research field, and impressive performance has been demonstrated for the storage of quantum states of light in gaseous [2] and in solid-state atomic ensembles [3–5]. Superconducting circuits resonate at microwave frequencies, and ensembles of electronic spins have been proposed as quantum memories in hybrid architectures for quantum computing including superconducting qubits [6–9]. Progress in this direction was reported in a number of experiments, demonstrating first strong coupling of an ensemble of spins in a crystal to a superconducting resonator [4,10–15], and more recently reversible storage of a single microwave photon in the spin ensemble [16,17]. From these results it clearly appears that inhomogeneous broadening of the spin ensemble is a major obstacle, which needs to be overcome for hybrid quantum circuits to fully benefit from the long spin-coherence times. Due to inhomogeneous broadening, quantum information leaks from the "bright" collective degree of freedom coupled to the cavity into dark modes of the spin ensemble [18–20]. An appealing possibility is to actively and coherently restore it using refocusing techniques, inspired from magnetic-resonance methods [21] and based on the application of π pulses to the spins acting as time reversal. However, these ideas face a number of challenges: (i) the spatial inhomogeneity of the microwave resonator field may make it difficult to apply a π pulse efficiently to each spin, (ii) after the π-pulse inversion, the spin ensemble should remain stable despite its coupling to the cavity, and (iii) the whole statistics of the collective spin must be restored at the single quantum level. The present work proposes a protocol, which addresses all these issues, and we exemplify its feasibility for the specific case of nitrogen vacancy (NV) centers in diamond [22], using currently available experimental techniques. The proposed memory extends the storage times by several orders of magnitude compared to Refs. [16,17]. It is intrinsically multimode and thus allows us to reversibly store a number of quantum states, paving the way to the realization of a genuine quantum Turing machine [7,23].

In our proposal the π pulses are performed by rapid adiabatic passage [24] through the electron spin resonance, a method known to tolerate an inhomogeneous microwave field. Stability of the ensemble against super-radiant decay after inversion is ensured provided the cavity quality factor is sufficiently low [25]. Since this is incompatible with a faithful transfer of quantum information from the cavity into the spins, we propose to use a cavity with a quality factor that can be tuned in between the steps of the protocol, as was recently demonstrated with SQUIDs [26]. In addition, inspired by a recent proposal of atomic-ensemble quantum memories for optical photons [5], we employ two π pulses in the refocusing scheme. To avoid emitting a microwave echo from the inverted spin ensemble, which would otherwise be more noisy than the original quantum state [27], we detune the cavity from the spins in between the two pulses (effectively "silencing" this noisy first echo [5]). The second echo, formed in a noninverted ensemble, restores the quantum information.

The proposed physical setup is shown schematically in Figs. 1(a) and 1(b); a diamond crystal containing NV centers [22] is placed on top of a transmission waveguide cavity whose frequency ω_c [26] and coupling to the measuring line κ [28] can be tuned on a nanosecond time scale using control lines (not shown in Fig. 1). The crystal is subjected to a constant bias magnetic field $\mathbf{B}_{\mathrm{NV}}$, lifting the degeneracy of the $m_S = \pm 1$ states, and bringing the $0 \rightarrow 1$ transition to an average frequency $\omega_s = 2\pi \times 2.9$ GHz. In the frame rotating at ω_s the free evolution of the cavity field and the spin ensemble is described by the Hamiltonian $\hat{H}_0 = \Delta_{cs}\hat{a}_c^\dagger \hat{a}_c + \sum_j \Delta_j \hat{\sigma}_z^{(j)}/2$, where $\hat{a}_c$ is the cavity field annihilation operator, $\Delta_{cs} = \omega_c - \omega_s$ is the (adjustable) spin-cavity detuning, $\Delta_j = \omega_j - \omega_s$, ω_j is the resonance frequency of the jth spin, and $\hat{\sigma}_z^{(j)}$ is the corresponding

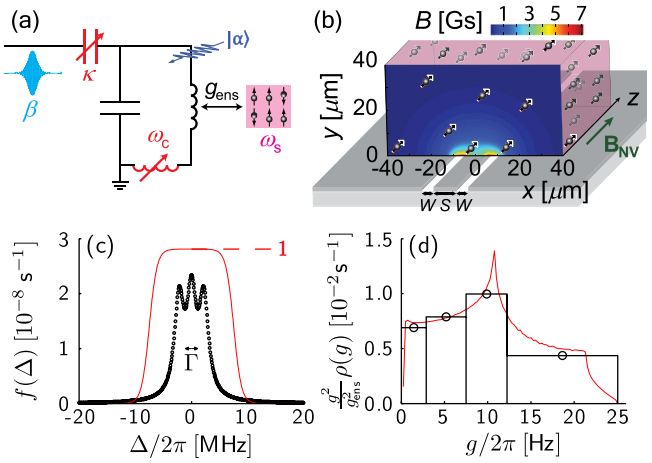

FIG. 1 (color online). (a) Quantum memory circuit. The resonator, with frequency ω_c and damping rate κ tunable at the nanosecond scale, is coupled to the spin ensemble (frequency ω_s) with an ensemble coupling constant $g_{\rm ens}$. Drive pulses of amplitude $\beta(t)$ are applied to the spins via the resonator, which can be initialized in a well-defined quantum state $|\alpha\rangle$. (b) Amplitude of the microwave field generated by a coplanar resonator with quality factor $Q = 100$ and driven by a pulse of 100 μW power. A static magnetic field $\mathbf{B}_{\rm NV}$ is applied parallel to the spins, which are distributed uniformly throughout the crystal. (c) Subensemble distribution $f(\Delta)$ of spin-resonance frequencies (circles) consisting of three hyperfine-split Lorentzian lines. The solid line shows the excitation probability for the chosen secant hyperbolic inversion pulses (see text). (d) The solid line shows calculated coupling-strength distribution function $\rho(g)g^2$. The histogram and circles show the subensemble distribution used in the calculation. The low- and high-frequency cutoffs in $\rho(g)$ originate from, respectively, high (40 μm) and low (0.5 μm) cutoffs in the distance from the resonator to NV centers.

Pauli operator. Nitrogen vacancy centers are coupled by hyperfine interaction to the nuclear spin of their nitrogen atom (having a spin 1), causing the $m_S = 0 \rightarrow 1$ transition to split into a triplet separated by $\Delta_{\rm hfs}/2\pi = 2.2$ MHz [29]. In addition, they are coupled by dipolar interactions to a bath of magnetic dipoles (see the Supplemental Material [30]), which is known to govern their coherence time [31–33]. This bath broadens each of the hyperfine resonances, with a Lorentzian line shape [32] of width w, corresponding to a free-induction decay time $T_2^* = 2/w$. A Hahn-echo pulse sequence [21] partially refocuses this coherence, yielding a coherence time T_2 which can be several orders of magnitude longer than T_2^*. In this work, we thus model the system by the static inhomogeneous spin distribution shown in Fig. 1(c) of characteristic width $\Gamma \approx w$ (see the Supplemental Material [30]), and damped at a rate $\gamma_\perp = T_2^{-1}$ in the Markov approximation (see the Supplemental Material [30]). The spin-cavity interaction is described by $\hat{H}_{\rm I} = \sum_j g_j(\hat{\sigma}_+^{(j)}\hat{a}_c + \hat{\sigma}_-^{(j)}\hat{a}_c^\dagger)$, where the coupling constant g_j of the jth spin is distributed as shown in Fig. 1(d) (see the Supplemental Material [30]).

This distribution is of no concern for storing the quantum state [16]; however, it prevents the application of a "hard" π pulse since each spin has a different Rabi frequency for a given drive amplitude. So-called hyperbolic secant pulses [34], where the pulse amplitude and phase are modulated as $a_c = a_c^{\rm max}[{\rm sech}(\beta_{\rm sech}t)]^{1+i\mu}$, are known to remedy this issue [35]. The pulses are applied by an external drive β modeled by the Hamiltonian $\hat{H}_{\rm ext} = i\sqrt{2\kappa}(\beta\hat{a}_c^\dagger - \beta^*\hat{a}_c)$. Note that to achieve the desired temporal dependence of $\hat{a}_c$, β must be further tailored in order to account for the cavity filtering and the coupling to the spins (see the Supplemental Material [30]).

The quantum memory protocol, shown schematically in Fig. 2(a), aims to store a cavity-field state given at $t = 0$ and retrieve it again at $t = T_{\rm mem}$ with the cavity tuned to a "target frequency" $\Delta_{cs}^{\rm t}$. This quantum state could be delivered by, e.g., a superconducting transmon qubit along the lines of Ref. [16]. The cavity state is then transferred to the spins by setting $\Delta_{cs} = 0$ for a time $T_{\rm swap}$ after which the cavity is parked at Δ_{cs}^{p}. In a lowest-order approximation $T_{\rm swap} = \pi/2g_{\rm ens}$ where $g_{\rm ens} = [\int g^2\rho(g)dg]^{1/2}$ corresponds to the resonator-spin ensemble swap rate [16,17,20], but in reality is optimized numerically. For a high-fidelity storage, we set $\kappa = \kappa_{\rm min} = \omega_c/2Q_{\rm max}$ with $Q_{\rm max} = 10^4$ so that the

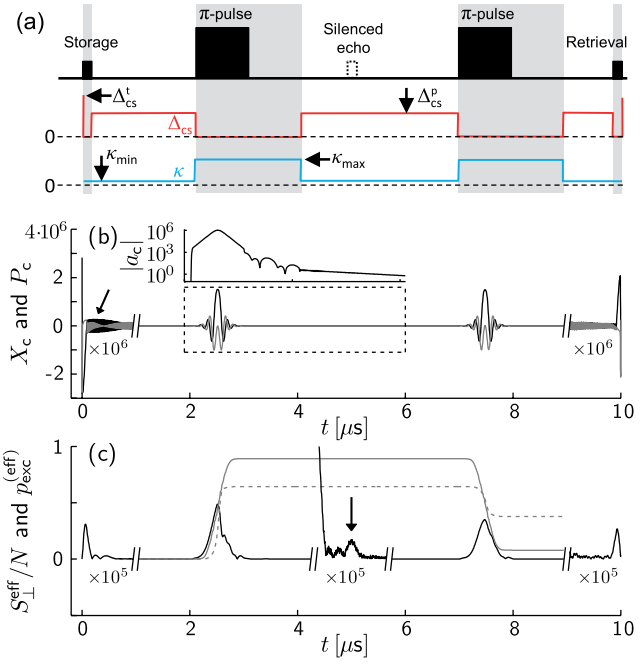

FIG. 2 (color online). (a) Schematic timing of pulses and cavity parameters Δ_{cs} and κ. Periods of resonance ($\Delta_{cs} = 0$) are marked by gray areas. (b) Cavity-field mean values X_c (black) and P_c (gray) versus time. The inset replots the dashed-line region with $|\langle\hat{a}_c\rangle|$ on the logarithmic vertical scale. (c) The g-weighted transverse-spin-component mean value $S_\perp^{\rm eff} = \sqrt{S_x^{\rm eff2} + S_y^{\rm eff2}}$ (black) normalized to N, the excitation probability $p_{\rm exc}$ (gray, dashed curve), and the g-weighted excitation probability $p_{\rm exc}^{\rm eff}$ (gray, solid curve).

spin ensemble and resonator are in strong coupling. Next, in order to refocus the reversible spin dephasing we apply two π pulses at $\sim T_{\rm mem}/4$ and $\sim 3T_{\rm mem}/4$ with $\Delta_{cs} = 0$, and to stabilize the inverted spin ensemble, we set $\kappa = \kappa_{\rm max} = \omega_c/2Q_{\rm min}$ with $Q_{\rm min} = 100$ before the π pulses so that the effective cooperativity parameter fulfills $C = g_{\rm ens}^2/\kappa\Gamma < 1$ [25]. An additional constraint comes from the fact that tuning the cavity frequency or quality factor with SQUIDs is possible only if the cavity field is sufficiently low ($|\langle \hat{a}_c \rangle| \lesssim 10$), which requires sufficient delay to allow it to decay after the π pulses. Between the two π pulses, we set $\Delta_{cs} = \Delta_{cs}^p$ in order to silence the first spin echo [5]. After the second π pulse the quantum state is retrieved from the spin ensemble by setting $\Delta_{cs} = 0$ during $T_{\rm swap}$ after which the cavity is tuned to $\Delta_{cs}^{\rm t}$.

The numerical calculation of the dynamical evolution is made tractable by dividing the spins into M subensembles along the lines of Ref. [25] keeping account of the mean values and covariances between cavity-field quadratures $\hat{X}_c = (\hat{a}_c + \hat{a}_c^\dagger)/\sqrt{2}$ and $\hat{P}_c = -i(\hat{a}_c - \hat{a}_c^\dagger)/\sqrt{2}$, and spin components $\hat{S}_k^{(m)} = \sum_{\mathcal{M}_m} \hat{\sigma}_k^{(j)}$, of the mth subensemble $\mathcal{M}_m$ with $k = x, y, z$ (see the Supplemental Material [30]). Such a representation is convenient for determining the memory performance for, e.g., coherent input states. Specific for our NV-center example we use $g_{\rm ens} = 2\pi \times 3.5$ MHz, $w = 2\pi \times 2$ MHz corresponding to $T_2^* = 0.16\,\mu$s, $T_2 = 100\,\mu$s (see the Supplemental Material [30]), an infinite population decay time, and hyperbolic secant π pulses truncated at a duration of 1 μs with $\mu = 3.5$ (practically making the inversion curve in Fig. 1(c) flat over the inhomogeneous distribution), and $\mu\beta_{\rm sech} = 2\pi \times 7.5$ MHz. We assume that a microwave drive of peak power up to 100 μW can be applied to the sample input without causing too much heating.

Typical results of our calculations are shown in Fig. 2. Figure 2(b) shows the mean values of $\hat{X}_c$ and $\hat{P}_c$ when a weak coherent cavity-field state is given at $t = 0$. Even though the cavity field is very strong during the inversion pulses at $t \approx 2.5$ μs and $t \approx 7.5$ μs, it relaxes to negligible levels prior to memory retrieval. Due to an imperfect storage process [marked by the arrow in Fig. 2(b)] a minor part of the field is left in the cavity (14% in field strength or 2% in energy units), but most importantly $|\langle \hat{a}_c \rangle|$ recovers at $t = T_{\rm mem}$ a value comparable to the one at $t = 0$. Regarding the spin state, we consider the effective, g-weighted spin observables $\hat{S}_\eta^{\rm eff} = \sum_j \hat{\sigma}_\eta^{(j)} g_j/\bar{g}$, with $\eta = x$, y and $\bar{g} = g_{\rm ens}/\sqrt{N}$, which couple directly to the cavity field $\hat{a}_c$ through the interaction Hamiltonian $\hat{H}_{\rm I}$. Figure 2(c) shows the magnitude of these transverse spin components; in the storage part it grows as the quantum state is swapped from the cavity and then decays within T_2^* due to inhomogeneous broadening. Despite the excitation of very large mean spin components by the π pulses, the much weaker mean values of the stored spin states are recovered as a primary echo [arrow in Fig. 2(c)] and at the final memory retrieval. Figure 2(c) also shows the excitation probability $p_{\rm exc} = (S_z + N)/2N$ and the effective, g-weighted excitation probability $p_{\rm exc}^{\rm eff} = (\sum_j \hat{\sigma}_z^{(j)} g_j^2/\bar{g}^2 + N)/2N$ versus time. The latter reaches 89% between inversion pulses and levels off at 8% after the second inversion pulse.

The above results can be extracted from mean-value equations alone and demonstrate the feasibility of the spin ensemble as a classical memory. In order to assess the quantum properties of the memory we also calculate the evolution of variances by the coupled first- and second-moment equations detailed in the Supplemental Material [30] (see Fig. 3). Figure 3(a) shows the summed variance of $\hat{X}_c$ and $\hat{P}_c$, which deviates from the coherent-state value of unity during inversion pulses. At the memory retrieval the variance also increases when the cavity is tuned to resonance with $Q = Q_{\rm max}$ due to emission from spins left in the excited state by a nonperfect inversion process (in analogy to Ref. [27]), but most importantly this excess noise of only 11% maintains easily the quantum nature of the memory.

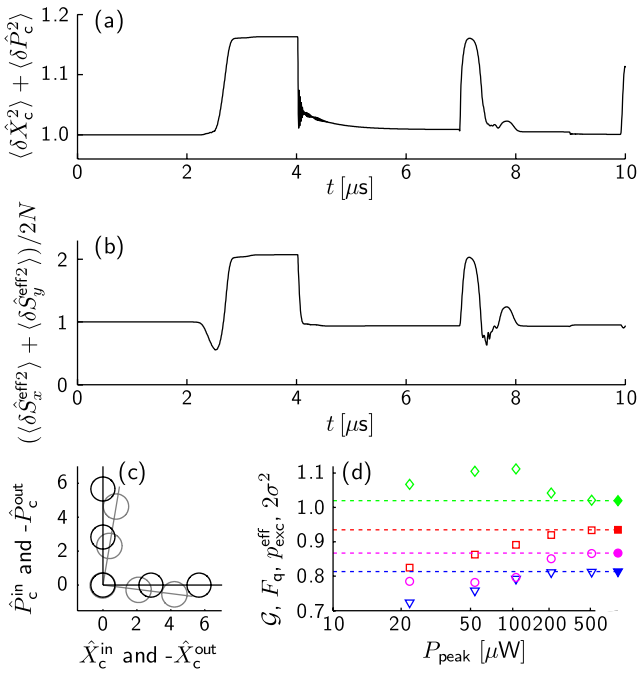

FIG. 3 (color online). (a) Summed variance of cavity-field quadratures. (b) The summed, g-weighted spin-component variance normalized to $2N$. (c) Various input states (black) and output states (gray, sign reversed) examined in the protocol. The centers of circles mark mean values whereas the radii mark the standard deviation σ of the state. (d) Open symbols: the dependence of gain $\mathcal{G}$ (blue triangles), qubit fidelity F_q (magenta circles), effective excitation probability $p_{\rm exc}^{\rm eff}$ (red squares), and summed variance $2\sigma^2$ (green diamonds) on the peak power $P_{\rm peak}$ of the external driving field during inversion pulses. Closed symbols: simulations with $P_{\rm peak} = 100$ μW and homogeneous coupling $g = 2\pi \times 12.5$ Hz, leading to $\mathcal{G} = 0.82$, $2\sigma^2 = 1.02$, and $F_q = 87\%$.

Figure 3(b) shows the summed variance of the spin components $\hat{S}_x^{\text{eff}}$ and $\hat{S}_y^{\text{eff}}$, which relaxes almost to the coherent-state value at the memory retrieval.

We note one advantageous property of the spin-frequency inhomogeneity: for a resonant cavity in low-Q mode the effective cooperativity parameter becomes $C = g_{\text{ens}}^2/\kappa_{\max}\Gamma \approx 0.38$. According to Ref. [25] this ensures (i) that the excess variance of $\hat{X}_c$, $\hat{P}_c$, $\hat{S}_x^{\text{eff}}$, and $\hat{S}_y^{\text{eff}}$ converge to moderate, finite values during the resonant, inverted period (see, e.g., Figs. 3(a) and 3(b) at 3 μs $\lesssim t \lesssim$ 4 μs), and (ii) that mean values of the coupled spin-cavity system observables relax sufficiently fast from possibly imperfect π pulses as exemplified in the inset of Fig. 2(b). For the off-resonant cavity the first and second moments of the spin components are damped on the T_2^* time scale as seen in Fig. 2(c) prior to the primary echo and in Fig. 3(b) at $t \approx 4$ μs, respectively. This is essential for the performance of the protocol; any reminiscence of the inversion pulses and excess noise in the spin ensemble must vanish both at the time of the primary echo and of the memory retrieval.

To assess the performance of the quantum memory, we repeat the above simulation with various other coherent input states. A selection of these are shown in Fig. 3(c) in terms of retrieved mean values and variances (gray circles) as compared to those of the input states (black circles). We confirm that the input-output relations constitute a linear map, which (i) essentially maps vacuum to vacuum (with a slightly increased variance) demonstrating that the remains of the inversion pulses are negligible, and (ii) presents a gain factor $\mathcal{G} = 0.79$ for the mean values. The quadrature variances of the retrieved states amount to $2\sigma^2 = \langle \delta\hat{X}_c^2 \rangle + \langle \delta\hat{P}_c^2 \rangle = 1.11$. Since any quantum state can be expressed as a superposition of coherent states the memory should work for arbitrary input states, e.g., cat states [36], and qubit states encoded in the $|0\rangle$ and $|1\rangle$ Fock states of the cavity. The storage time depends on the quantum state and the desired fidelity. Following Ref. [37] we obtain a qubit fidelity $F_q = 80\%$ for $T_{\text{mem}} = 10$ μs.

To investigate the implications of the limited peak power available for inversion pulses, the above-mentioned analysis is repeated for a selection of peak powers ranging from 20 to 500 μW leading to the results presented in Fig. 3(d) with open symbols. Furthermore, a simulation is carried out at $P_{\text{peak}} = 100$ μW but with a homogeneous distribution of coupling strengths $g/2\pi = 12.5$ Hz [solid symbols in Fig. 3(d)]. Clearly, increasing P_{peak} presents an increase in $\mathcal{G}$ due to a better inversion process, but since in an intermediate regime a fraction of spins experiences a poor inversion process due to insufficient Rabi frequency [limiting the inversion performance illustrated by the dashed curve in Fig. 2(c)] we observe the nonmonotonic behavior of $2\sigma^2$ shown in Fig. 3(d). While increasing driving powers may be infeasible from an experimental point of view an alternative route to improvement lies in tailoring a more homogeneous distribution of coupling strengths, e.g., by limiting the distance between NV centers and the cavity.

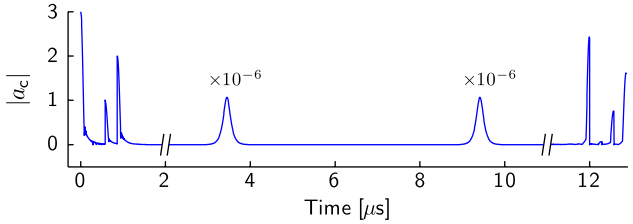

FIG. 4 (color online). The cavity field $|a_c|$ versus time in a multimode storage example with four input fields ($|a_c| = 3, 0, 1, 2$) separated by 0.29 μs, with memory time 12 μs. The amplitude cross talk is below 3%.

Continuing the analysis with a homogeneous coupling-strength distribution [solid symbols in Fig. 3(d), $F_q = 87\%$], we find the limiting factors for the obtained fidelity, which in terms of gain can be written approximately as $\mathcal{G} = \mathcal{G}_0 \exp(-\kappa[\pi/2g_{\text{ens}} + 2T_{\text{chirp}}]) \exp(-\gamma_\perp[T_{\text{mem}} - 0.7\ \mu\text{s}])$. The κ-dependent factor yields ≈ 0.92 due to cavity decay during the resonant swapping process and during the initial and final frequency chirp of duration T_{chirp}. The $\gamma_\perp$-dependent factor yields ≈ 0.91 due to spin decoherence (partly suppressed when the quantum state resides in the cavity or a population degree of freedom). The main contribution to excess noise arises from imperfect inversion processes, e.g., due to the dephasing rate $\gamma_\perp$ during π pulses. In the limit T_2, $Q_{\max} \to \infty$ the qubit fidelity becomes $\approx 97\%$, and the origin of the remaining infidelity ($\mathcal{G}_0 \approx 0.97$ and $2\sigma^2 \approx 1.01$) includes a nonperfect cavity-to-spin transfer [arrow in Fig. 2(b)] and residual imperfections in the inversion processes.

As demonstrated experimentally for classical pulses [38], the spin-ensemble quantum memory is multimode in nature, which we confirm by simulating the storage and retrieval of four pulses (see Fig. 4). The number of storage modes (proportional to T_2^*/T_2) that can be faithfully addressed and refocused is estimated to be $\sim$100 (see the Supplemental Material [30]).

In summary, a multimode spin-ensemble-based quantum memory for cavity fields has been proposed and analyzed for a specific realization using NV centers in diamond. To outperform classical memory strategies a fidelity of $F_q > 2/3$ is required, which is indeed predicted by our analysis for $T_{\text{mem}} \leq 69$ μs with present-day experimental parameters. The protocol could be modified to include dynamical decoupling pulse sequences [39]. Polarizing the ensemble nuclear spin would both improve the fidelity of the refocusing pulses and enable quantum state transfer from the electron to the nuclear spins [40]. In that way, second-long [41] multimode storage of microwave photons would be within reach.

The authors acknowledge useful discussions with T. Chanelière, D. Esteve, and Y. Kubo and support from

the EU integrated project AQUTE, the EU 7th Framework Programme collaborative project iQIT, and the ANR project QINVC (CHIST-ERA program).

Note added.—A similar memory protocol for propagating micro-wave photons is discussed in Ref. [42].

*brianj@phys.au.dk

[1] C. Simon *et al.*, Eur. Phys. J. D **58**, 1 (2010).
[2] K. Hammerer, A. S. Sørensen, and E. S. Polzik, Rev. Mod. Phys. **82**, 1041 (2010).
[3] W. Tittel, M. Afzelius, T. Chanelière, R. L. Cone, S. Kröll, S. A. Moiseev, and M. Sellars, Laser Photonics Rev. **4**, 244 (2010).
[4] M. U. Staudt, I.-C. Hoi, P. Krantz, M. Sandberg, M. Simoen, P. Bushev, N. Sangouard, M. Afzelius, V. S. Shumeiko, G. Johansson, P. Delsing, and C. M. Wilson, J. Phys. B **45**, 124019 (2012).
[5] V. Damon, M. Bonarota, A. Louchet-Chauvet, T. Chanelière, and J.-L. Le Gouët, New J. Phys. **13**, 093031 (2011).
[6] A. Imamoglu, Phys. Rev. Lett. **102**, 083602 (2009).
[7] J. H. Wesenberg, A. Ardavan, G. A. D. Briggs, J. J. L. Morton, R. J. Schoelkopf, D. I. Schuster, and K. Mølmer, Phys. Rev. Lett. **103**, 070502 (2009).
[8] D. Marcos, M. Wubs, J. M. Taylor, R. Aguado, M. D. Lukin, and A. S. Sørensen, Phys. Rev. Lett. **105**, 210501 (2010).
[9] W. L. Yang, Z. Q. Yin, Y. Hu, M. Feng, and J. F. Du, Phys. Rev. A **84**, 010301(R) (2011).
[10] Y. Kubo, F. R. Ong, P. Bertet, D. Vion, V. Jacques, D. Zheng, A. Dreau, J. F. Roch, A. Auffeves, F. Jelezko, J. Wrachtrup, M. F. Barthe, P. Bergonzo, and D. Esteve, Phys. Rev. Lett. **105**, 140502 (2010).
[11] D. I. Schuster, A. P. Sears, E. Ginossar, L. DiCarlo, L. Frunzio, J. J. L. Morton, H. Wu, G. A. D. Briggs, B. B. Buckley, D. D. Awschalom, and R. J. Schoelkopf, Phys. Rev. Lett. **105**, 140501 (2010).
[12] R. Amsüss, C. Koller, T. Nöbauer, S. Putz, S. Rotter, K. Sandner, S. Schneider, M. Schramböck, G. Steinhauser, H. Ritsch, J. Schmiedmayer, and J. Majer, Phys. Rev. Lett. **107**, 060502 (2011).
[13] H. Huebl, C. Zollitsch, J. Lotze, F. Hocke, M. Greifenstein, A. Marx, R. Gross, and S. T. B. Goennenwein, arXiv:1207.6039.
[14] V. Ranjan, G. de Lange, R. Schutjens, T. Debelhoir, J. P. Groen, D. Szombati, D. J. Thoen, T. M. Klapwijk, R. Hanson, and L. DiCarlo, Phys. Rev. Lett. **110**, 067004 (2013).
[15] S. Probst, H. Rotzinger, S. Wünsch, P. Jung, M. Jerger, M. Siegel, A. V. Ustinov, and P. A. Bushev, Phys. Rev. Lett. **110**, 157001 (2013).
[16] Y. Kubo, C. Grezes, A. Dewes, T. Umeda, J. Isoya, H. Sumiya, N. Morishita, H. Abe, S. Onoda, T. Ohshima, V. Jacques, A. Dréau, J.-F. Roch, I. Diniz, A. Auffeves, D. Vion, D. Esteve, and P. Bertet, Phys. Rev. Lett. **107**, 220501 (2011).
[17] X. Zhu, S. Saito, A. Kemp, K. Kakuyanagi, S.-i. Karimoto, H. Nakano, W. J. Munro, Y. Tokura, M. S. Everitt, K. Nemoto, M. Kasu, N. Mizuochi, and K. Semba, Nature (London) **478**, 221 (2011).
[18] Z. Kurucz, J. H. Wesenberg, and K. Mølmer, Phys. Rev. A **83**, 053852 (2011).
[19] I. Diniz, S. Portolan, R. Ferreira, J. M. Gérard, P. Bertet, and A. Auffèves, Phys. Rev. A **84**, 063810 (2011).
[20] Y. Kubo, I. Diniz, A. Dewes, V. Jacques, A. Dréau, J.-F. Roch, A. Auffeves, D. Vion, D. Esteve, and P. Bertet, Phys. Rev. A **85**, 012333 (2012).
[21] E. L. Hahn, Phys. Rev. **80**, 580 (1950).
[22] A. Gruber, A. Dräbenstedt, C. Tietz, L. Fleury, J. Wrachtrup, and C. von Borczyskowski, Science **276**, 2012 (1997).
[23] K. Tordrup, A. Negretti, and K. Mølmer, Phys. Rev. Lett. **101**, 040501 (2008).
[24] A. Abragam, *The Principles of Nuclear Magnetism* (Clarendon, Oxford, 1961).
[25] B. Julsgaard and K. Mølmer, Phys. Rev. A **86**, 063810 (2012).
[26] A. Palacios-Laloy, F. Nguyen, F. Mallet, P. Bertet, D. Vion, and D. Esteve, J. Low Temp. Phys. **151**, 1034 (2008).
[27] J. Ruggiero, J.-L. Le Gouët, C. Simon, and T. Chanelière, Phys. Rev. A **79**, 053851 (2009).
[28] Y. Yin, Y. Chen, D. Sank, P. J. J. O'Malley, T. C. White, R. Barends, J. Kelly, E. Lucero, M. Mariantoni, A. Megrant, C. Neill, A. Vainsencher, J. Wenner, A. N. Korotkov, A. N. Cleland, and J. M. Martinis, Phys. Rev. Lett. **110**, 107001 (2013).
[29] S. Felton, A. M. Edmonds, M. E. Newton, P. M. Martineau, D. Fisher, D. J. Twitchen, and J. M. Baker, Phys. Rev. B **79**, 075203 (2009).
[30] See Supplemental Material at http://link.aps.org/supplemental/10.1103/PhysRevLett.110.250503 for technical details on the experimental proposal and theoretical analysis.
[31] R. Hanson, V. V. Dobrovitski, A. E. Feiguin, O. Gywat, and D. D. Awschalom, Science **320**, 352 (2008).
[32] V. V. Dobrovitski, A. E. Feiguin, D. D. Awschalom, and R. Hanson, Phys. Rev. B **77**, 245212 (2008).
[33] N. Zhao, S.-W. Ho, and R.-B. Liu, Phys. Rev. B **85**, 115303 (2012).
[34] M. S. Silver, R. I. Joseph, and D. I. Hoult, Phys. Rev. A **31**, R2753 (1985).
[35] M. Garwood and L. DelaBarre, J. Magn. Reson. **153**, 155 (2001).
[36] H. Wang, M. Hofheinz, M. Ansmann, R. C. Bialczak, E. Lucero, M. Neeley, A. D. OConnell, D. Sank, M. Weides, J. Wenner, A. N. Cleland, and J. M. Martinis, Phys. Rev. Lett. **103**, 200404 (2009).
[37] J. F. Sherson, H. Krauter, R. K. Olsson, B. Julsgaard, K. Hammerer, I. Cirac, and E. S. Polzik, Nature (London) **443**, 557 (2006).
[38] H. Wu, R. E. George, J. H. Wesenberg, K. Mølmer, D. I. Schuster, R. J. Schoelkopf, K. M. Itoh, A. Ardavan, J. J. L. Morton, and G. A. D. Briggs, Phys. Rev. Lett. **105**, 140503 (2010).
[39] G. de Lange, Z. H. Wang, D. Ristè, V. V. Dobrovitski, and R. Hanson, Science **330**, 60 (2010).
[40] G. D. Fuchs, G. Burkard, P. V. Klimov, and D. D. Awschalom, Nat. Phys. **7**, 789 (2011).
[41] N. Bar-Gill, L. M. Pham, A. Jarmola, D. Budker, and R. L. Walsworth, arXiv:1211.7094.
[42] M. Afzelius, N. Sangouard, G. Johansson, M. U. Staudt, and C. M. Wilson, arXiv:1301.1858.